Magnetic dipole excitations based on the relativistic nuclear energy density functional

G. Kružić*
Department of Physics, Faculty of Science, University of Zagreb, Bijenička cesta 32, HR-10000, Zagreb, Croatia and Research Department, Ericsson-Nikola Tesla, Krapinska 45, HR-10000, Zagreb, Croatia

T. Oishi,† D. Vale,‡ and N. Paar§
Department of Physics, Faculty of Science, University of Zagreb, Bijenička c. 32, HR-10000, Zagreb, Croatia

(Received 4 March 2020; revised 22 April 2020; accepted 23 September 2020; published 13 October 2020)

Magnetic dipole ($M1$) excitations constitute not only a fundamental mode of nucleonic transitions, but they are also relevant for nuclear astrophysics applications. We have established a theory framework for the description of $M1$ transitions based on the relativistic nuclear energy density functional. For this purpose, the relativistic quasiparticle random phase approximation (RQRPA) is established using density-dependent point coupling interaction DD-PC1, supplemented with the isovector-pseudovector interaction channel in order to study unnatural parity transitions. The introduced framework has been validated using the $M1$ sum rule for core-plus-two-nucleon systems, and employed in studies of the spin, orbital, isoscalar, and isovector $M1$ transition strengths that relate to the electromagnetic probe in magic nuclei ^{48}Ca and ^{208}Pb and open shell nuclei ^{42}Ca and ^{50}Ti. In these systems, the isovector spin-flip $M1$ transition is dominant, mainly between one or two spin-orbit partner states. It is shown that pairing correlations have a significant impact on the centroid energy and major peak position of the $M1$ mode. The $M1$ excitations could provide an additional constraint to improve nuclear energy density functionals in the future studies.

DOI: 10.1103/PhysRevC.102.044315

I. INTRODUCTION

Electromagnetic excitations in finite nuclei represent one of the most important probes of relevance in nuclear structure and dynamics, as well as in nuclear astrophysics. In particular, various aspects of magnetic dipole ($M1$) mode have been considered both in experimental and theoretical studies [1–8] due to its relevance for diverse nuclear properties associated, e.g., to unnatural parity states, spin-orbit splittings, and tensor force effects. Specifically, $M1$ spin-flip excitations are analogs of Gamow-Teller (GT) transitions, meaning that, at the operator level, the dominant $M1$ isovector component is the synonym for the zeroth component of GT transitions and can serve as probe for calculations of inelastic neutrino-nucleus cross section [9,10]. This process is hard to measure but it is essential in supernova physics, as well as in the r-process nucleosynthesis calculations [7,8,11,12]. The isovector spin-flip $M1$ response is also relevant for applications related to the design of nuclear reactors [13], for the understanding of single-particle properties, spin-orbit interaction, and shell closures from stable nuclei toward limits of stability [14–18], as well as for the resolving the problem of quenching of the spin-isopin response in nuclei that is necessary for a reliable description of double-β decay matrix elements [19]. In deformed nuclei, another type of $M1$ excitations has been extensively studied, known as scissors mode, where the orbital part of the $M1$ operator plays a dominant role in a way that protons and neutrons oscillate with opposite phase around the core [3,20–28].

In any nuclei undergoing experimental investigation, there are simultaneously present $E\lambda$ and $M\lambda$ multipole excitations, where the electric dipole ($E1$) and electric quadrupole ($E2$) responses [29–34] dominate over the $M1$ response [35–43]. Thus, it is a rather challenging task to measure $M1$-related observables in a whole energy range. Even for the nuclides accessible by experiments, their full information on the $M1$ response has not been complete.

The $M1$ transitions have been studied in various theoretical approaches. Various aspects of the $M1$ mode have been investigated in the shell model [9,12,14,15,22,44,45], including, e.g., scissors and unique-parity modes [22], tensor-force effect [14], low-energy enhancement of radiation [44], and the analogy with neutrino-nucleus scattering [9,12]. The $M1$ energy-weighted sum rule has been discussed from a perspective of the spin-orbit energy [46]. The Landau-Migdal interaction has been one of the relevant topics in studies of $M1$ excitations [47,48]. In order to reproduce a large fragmentation of the experimental $M1$ strength, the importance of including complex couplings going beyond the RPA level has also been addressed [26,47–50].

Recently, the $M1$ excitation has been investigated in the framework based on the Skryme functionals [16–18], also

*goran.kruzic@ericsson.com
†toishi@phy.hr
‡denivalesq@gmail.com
§npaar@phy.hr

extended to include tensor effects [51]. It has been shown that the results for the spin-flip resonance obtained by using different parametrizations do not appear as convincing interpretation of the experimental results. Additional effects have been explored in order to resolve this issue, e.g., the isovector-$M1$ response versus isospin-mixed responses, and the role of tensor and vector spin-orbit interactions [16,17]. In recent analysis in Ref. [52], based on the Skyrme functionals, it has been shown that while modern Skyrme parametrizations successfully reproduce electric excitations, there are difficulties to describing magnetic transitions. In addition, some Skyrme sets result in the ambiguity that, by the same parametrization, the model cannot simultaneously describe one-peak and two-peak data for closed and open shell nuclei [16]. Thus, further developments of the Skyrme functional in the spin channel are called for [52]. Simultaneously, it is essential to explore the $M1$ response from different theoretical approaches to achieve a complete understanding of their properties, as well as to assess the respective systematic uncertainties.

The aim of this work is to describe the properties of $M1$ excitations from a different perspective, by implementing a theoretical framework derived from the relativistic nuclear energy density functional. In the past, this framework has been successfully employed to describe a variety of nuclear properties and astrophysically relevant processes [53–66]. In open shell nuclei, the pairing correlations make non-negligible contributions to the properties of $M1$ transitions [29,67], and thus they are also included in model calculations.

The paper is organized as follows. In Sec. II, the overview of the formalism of the relativistic quasiparticle random phase approximation (QRPA) for magnetic transitions based on the relativistic point-coupling interaction is given. Section II C is devoted to display the benchmark result of our relativistic QRPA scheme in comparison with the sum rule in Ref. [29]. The results of model calculations and comparison with the experimental studies are presented in Secs. III A and III B, while the pairing effects are considered in Sec. III C. A summary of the present work is given in Sec. IV.

II. FORMALISM

We study $M1$ excitations based on particle-hole (1p-1h) (or in open shell nuclei two-quasiparticle) transitions from 0^+ ground state (GS) to 1^+ excited states of even-even nuclei within the formalism of a relativistic nuclear energy density functional (RNEDF), assuming the spherical symmetry [65]. More details about the RNEDF and its implementations are given in Refs. [65,68]. In this work, the nuclear ground state has been calculated by employing the self-consistent relativistic Hartree-Bogoliubov (RHB) model [65], where the mean field is derived for the relativistic point-coupling interaction with density-dependent couplings. Many effects that go beyond the mean-field level are not explicitly included in the RHB model, e.g., Fock terms, vacuum polarization effects, and the short-range Brueckner-type correlations. Since the parameters of the RNEDF are adjusted to the experimental data which contain all these and other effects, it means that effects beyond the mean-field level are implicitly included in the RHB approach by adjusting the model parameters to reproduce a selected empirical data set [53]. The no-sea approximation is also employed for relativistic mean-field calculations [53].

Here we briefly present the formalism of the relativistic point coupling interaction starting from the Lagrangian density,

$$\begin{aligned}\mathcal{L} = &\bar{\Psi}_N(i\gamma^\mu\partial_\mu - m_{0N})\Psi_N \\ &- \frac{1}{2}\alpha_S(\rho)(\bar{\Psi}_N\Psi_N)(\bar{\Psi}_N\Psi_N) \\ &- \frac{1}{2}\alpha_V(\rho)(\bar{\Psi}_N\gamma^\nu\Psi_N)(\bar{\Psi}_N\gamma_\nu\Psi_N) \\ &- \frac{1}{2}\alpha_{TV}(\rho)(\bar{\Psi}_N\vec{\tau}\gamma^\nu\Psi_N)(\bar{\Psi}_N\vec{\tau}\gamma_\nu\Psi_N) \\ &- \frac{1}{2}\delta_S(\partial_\nu\bar{\Psi}_N\Psi_N)(\partial^\nu\bar{\Psi}_N\Psi_N) \\ &- e\bar{\Psi}_N(\gamma^\nu A_\nu(\vec{x}))\frac{1-\hat{\tau}_3}{2}\Psi_N. \end{aligned} \tag{1}$$

The first term corresponds to the free nucleon field of Dirac type, while the point coupling interaction terms include isoscalar-scalar ($J^\pi = 0^+$), isoscalar-vector ($J^\pi = 1^-$), and isovector-vector ($J^\pi = 1^-$) channels (where J denotes the quantum number for the angular momentum and π denotes the parity), coupling of protons to the electromagnetic field, and the derivative term accounting for the leading effects of finite-range interactions necessary for a quantitative description of nuclear density distribution and radii.

The density-dependent couplings in each channel, $\alpha_S(\rho)$ (isoscalar-scalar), $\alpha_V(\rho)$ (isoscalar-vector), and $\alpha_{TV}(\rho)$ (isovector-vector), are modeled by the well-behaved functional [65],

$$\alpha_i(\rho) = a_i + (b_i + c_i x)e^{-d_i x}, \tag{2}$$

where $x = \frac{\rho}{\rho_{\text{sat.}}}$ and $\rho_{\text{sat.}}$ denotes nucleon density at saturation point for the case of symmetric nuclear matter. The respective parameters for each channel $i = S, V, TV$ are denoted as a_i, b_i, c_i, and s_i, while δ_S denotes the strength of isoscalar-scalar derivative term. In this work, the DD-PC1 parametrization is used in model calculations [65]. The RHB model employed in this study includes pairing correlations described by the pairing part of the phenomenological Gogny interaction [53],

$$V^{\text{pp}}(1,2) = \sum_{i=1,2} e^{[(r_1-r_2)/\mu_i]^2}(W_i + B_i\hat{P}^\sigma - H_i\hat{P}^\tau - M_i\hat{P}^\sigma\hat{P}^\tau), \tag{3}$$

where $\hat{P}^\sigma$ and $\hat{P}^\tau$ indicate the exchanges of the spin and isospin, respectively. The parameters μ_i, W_i, B_i, H_i, and M_i ($i = 1, 2$) are given by the D1S set as in Ref. [69]. We confirmed that, combined with the density dependent point coupling DD-PC1 functional for the mean-field part, this parametrization sufficiently reproduces the empirical pairing gaps of open shell systems in this study.

For the $M1$ excitations of nuclei, we utilize the relativistic quasiparticle random phase approximation (RQRPA) [70], which is in this work developed for the implementation of the relativistic point-coupling interaction, extended to describe the unnatural-parity transitions of the $M1$ type. In the limit

of small-amplitude oscillations, the RQRPA matrix equations read

$$\begin{pmatrix} A^J & B^J \\ B^{*J} & A^{*J} \end{pmatrix} \begin{pmatrix} X^{\nu,JM} \\ Y^{\nu,JM} \end{pmatrix} = \hbar\omega_\nu \begin{pmatrix} 1 & 0 \\ 0 & -1 \end{pmatrix} \begin{pmatrix} X^{\nu,JM} \\ Y^{\nu,JM} \end{pmatrix} \quad (4)$$

with $\hbar\omega_\nu = E_\nu - E_0$, where E_0 and E_ν are the RHB ground and excitation energies of the many-particle system, respectively. The X^ν and Y^ν indicate the forward-scattering and backward-scattering two-quasiparticle amplitudes. The particle-hole channel of the residual RQRPA interaction, V^{ph}, has been calculated by the effective Lagrangian from Eq. (1), but supplemented with the isovector-pseudovector interaction, as we explain in the following section. The RQRPA particle-particle correlations, V^{pp}, is evaluated from the Gogny-D1S force, which is commonly used in the RHB model.

The RHB calculations in this work are performed in the computational framework developed in Refs. [65,68,70,71]. The ground state of spherical nucleus is solved in the model space expanded in the harmonic oscillator (HO) basis, including up to 20 shells. The cutoff energies for the configuration space in the QRPA are selected to provide a sufficient convergence in the $M1$ excitation strength.

A. Isovector-pseudovector interaction

In order to describe the unnatural parity excitations of the $M1$ type ($J^\pi = 1^+$), the RQRPA residual interaction is further extended by introducing the relativistic isovector-pseudovector (IV-PV) contact interaction,

$$\mathcal{L}_{\text{IV-PV}} = -\tfrac{1}{2}\alpha_{\text{IV-PV}}[\bar{\Psi}_N\gamma^5\gamma^\mu\vec{\tau}\Psi_N][\bar{\Psi}_N\gamma^5\gamma_\mu\vec{\tau}\Psi_N]. \quad (5)$$

This pseudovector type of interaction has been modeled as a scalar product of two pseudovectors. The strength parameter for this channel, $\alpha_{\text{IV-PV}}$, is considered as a parameter, which is constrained by the experimental data on $M1$ transitions of selected nuclei. We note that the IV-PV term does not contribute in the RHB calculation of the ground state, and thus its strength parameter cannot be constrained together with other model parameters on the bulk properties of nuclear ground state. The pseudovector type of interaction would lead to the parity-violating mean field at the Hartree level for the description of the 0^+ nuclear ground state, and it contributes only to the RQRPA equations for unnatural parity transitions, i.e., 1^+ excitation of the $M1$ type.

The coupling strength parameter $\alpha_{\text{IV-PV}}$ is determined by minimizing the standard deviation $\sigma_\Delta(\alpha_{\text{IV-PV}})$, where Δ is the gap between the theoretically calculated centroid energy and experimentally determined dominant peak position of measured $M1$ transition strength in ^{208}Pb [38] and ^{48}Ca [37] nuclei. It turns out that the optimal parameter value is $\alpha_{\text{IV-PV}} = 0.53$ MeVfm^3 and in this case the energy gap Δ is less than 1 MeV both for ^{208}Pb and ^{48}Ca. In this way, all the parameters employed in the present analysis are constrained and further employed in the analysis of the properties of $M1$ excitations.

B. Transition strength for $M1$ excitations

In the following, we give an overview of the formalism for the transition strength for $M1$ transitions, for the implementation in the RQRPA. The transition strength for magnetic multipole excitations $B(MJ, \omega_\nu)$ can be distinguished to isoscalar strength $B^{(\text{IS})}(MJ, \omega_\nu)$, isovector strength $B^{(\text{IV})}(MJ, \omega_\nu)$, as well as spin $B^\sigma(MJ, \omega_\nu)$ and orbital $B^\ell(MJ, \omega_\nu)$ strengths. From the transition strength distribution of interest, the energy weighted moment m_k and centroid energy $\bar{E}$ can be calculated.

Within the (Q)RPA framework, discrete spectrum $B(MJ, \omega_\nu)$ of excited states is obtained. For demonstration purposes, this quantity is convoluted with the Lorentzian distribution [70],

$$R_{MJ}(E) = \sum_\nu B(MJ, \omega_\nu)\frac{1}{\pi}\frac{\Gamma/2}{(E - \hbar\omega_\nu)^2 + (\Gamma/2)^2}, \quad (6)$$

where the Lorentzian width is set as $\Gamma = 1.0$ MeV. The discrete strength $B(MJ, \omega_\nu)$ for the magnetic operator $\hat{\mu}_{JM}$ of rank J is, within the spherical assumption, calculated by the following expression [70],

$$\begin{aligned} B(MJ, \omega_\nu) = \Bigg| \sum_{\kappa\kappa'} \Big(& X^{\nu,J0}_{\kappa\kappa'}\langle\kappa||\hat{\mu}_J||\kappa'\rangle \\ & + (-1)^{j_\kappa - j_{\kappa'} + J} Y^{\nu,J0}_{\kappa\kappa'}\langle\kappa'||\hat{\mu}_J||\kappa\rangle\Big) \\ & \times (u_\kappa v_{\kappa'} + (-1)^J v_\kappa u_{\kappa'})\Bigg|^2, \end{aligned} \quad (7)$$

where κ and κ' are quantum numbers denoting single-particle states in the canonical basis [70]. u_κ and v_κ are the RHB occupation coefficients of single-particle states.

In the case of $M1$ excitations ($0^+ \to 1^+$), the rank of the transition operator is $J = 1$. The reduced matrix element for the $M1$ operator $\hat{\boldsymbol{\mu}}$, in mixed spin-isospin basis, is given by

$$\begin{aligned} & \langle j_f; t_f, t_{zf}||\hat{\boldsymbol{\mu}}||j_i; t_i, t_{zi}\rangle \\ & = \Bigg(\langle j_f||\hat{\boldsymbol{\mu}}^{(\text{IS})}||j_i\rangle\langle t_f||1_\tau||t_i\rangle \\ & \quad - \frac{C_{M1}}{\sqrt{2t_f + 1}}\langle j_f||\hat{\boldsymbol{\mu}}^{(\text{IV})}||j_i\rangle\langle t_f||\hat{\vec{\tau}}||t_i\rangle \Bigg), \end{aligned} \quad (8)$$

where the two resulting matrix elements correspond to the transitions of isoscalar and isovector type. Here $C_{M1} = \langle\frac{1}{2}t_z; 10|\frac{1}{2}t_z\rangle$ denotes Clebsch-Gordan coefficient in isospin space with convention $t_z = \frac{1}{2}$ for neutrons ($C_{M1} = \frac{1}{\sqrt{3}}$) and $t_z = -\frac{1}{2}$ for protons ($C_{M1} = -\frac{1}{\sqrt{3}}$).

A complete expression of the $M1$ operator in the relativistic formalism which acts on Hilbert space with mixed spin-isospin basis is given in a block diagonal form,

$$\begin{aligned} \hat{\boldsymbol{\mu}}_{1\nu} = & \sum_{k=1}^{A} \begin{pmatrix} \hat{\boldsymbol{\mu}}^{(\text{IS})}_{1\nu}(11)_k & 0 \\ 0 & \hat{\boldsymbol{\mu}}^{(\text{IS})}_{1\nu}(22)_k \end{pmatrix} \otimes 1_\tau \\ & - \sum_{k=1}^{A} \begin{pmatrix} \hat{\boldsymbol{\mu}}^{(\text{IV})}_{1\nu}(11)_k & 0 \\ 0 & \hat{\boldsymbol{\mu}}^{(\text{IV})}_{1\nu}(22)_k \end{pmatrix} \otimes \hat{\tau}_3, \end{aligned} \quad (9)$$

where 1_τ and $\hat{\tau}_3$ are units and Pauli's 2×2 matrices in isospin space. The $\hat{\boldsymbol{\mu}}^{(\text{IS})}_{1\nu}$ and $\hat{\boldsymbol{\mu}}^{(\text{IV})}_{1\nu}$ components correspond to the isoscalar and isovector parts of the $M1$ operator for the kth

nucleon, given by

$$\hat{\boldsymbol{\mu}}_{1\nu}^{(\mathrm{IS,IV})}(11)_k = \hat{\boldsymbol{\mu}}_{1\nu}^{(\mathrm{IS,IV})}(22)_k = \frac{\mu_N}{\hbar}\left(g_\ell^{\mathrm{IS,IV}}\hat{\boldsymbol{\ell}}_k + g_s^{\mathrm{IS,IV}}\hat{\mathbf{s}}_k\right)\cdot\boldsymbol{\nabla}(rY_{1\nu}(\Omega_k)). \quad (10)$$

The empirical gyromagnetic ratios for the bare proton (π) and neutron (ν) are given as $g_\ell^{\pi(\nu)} = 1\,(0)$ and $g_s^{\pi(\nu)} = 5.586\,(-3.826)$ [36], where the units are given in nuclear magnetons, $\mu_N = e\hbar/(2m_\mathrm{N})$.

In this work, so-called isoscalar and isovector gyromagnetic ratios are determined separately for the orbital and spin components [36,72]. That is,

$$g_\ell^{\mathrm{IS}} = \frac{g_\ell^\pi + g_\ell^\nu}{2} = 0.5, \quad g_s^{\mathrm{IS}} = \frac{g_s^\pi + g_s^\nu}{2} = 0.880, \quad (11)$$

and

$$g_\ell^{\mathrm{IV}} = \frac{g_\ell^\pi - g_\ell^\nu}{2} = 0.5, \quad g_s^{\mathrm{IV}} = \frac{g_s^\pi - g_s^\nu}{2} = 4.706. \quad (12)$$

This decomposition of the isoscalar and isovector $M1$ operators is consistent with the nonrelativistic formalism already used in previous studies, e.g., Refs. [36,72]. More details are given in the Appendix.

In the probe-independent consideration of nuclear excitations, the IS and IV operators have equal weights. In this manner, the IS or IV character is a structural feature of the nucleus, and it is independent of the probe, which can be either strong, electromagnetic, or weak [73]. In the present $M1$ case, the g_s factors in the IS and IV operators are different and are probe dependent [73,74]. Convention given in Eqs. (11) and (12) corresponds to the electromagnetic process [73]. As pointed out in Ref. [73], for the electromagnetic processes, the IS-spin g factor is considerably smaller than the IV one, i.e., $(g_s^{\mathrm{IS}}/g_s^{\mathrm{IV}})^2 \approx 1/30$, as one can see from the values given above. Note also that, for the hadronic processes, the IS-spin coupling is still smaller than the IV one, but with an enhancement at intermediate energy [73,74].

Previous studies also addressed possible quenching effects on the $M1$ mode. Several theoretical descriptions of the total $M1$ transition strength result in the overestimated values, in comparison to the experiments (see review in Ref. [22]). One phenomenological solution is to introduce the in-medium effects by quenching the gyromagnetic factors, $g_{s,\,\ell}$ [16,17,22]. In addition, experiments report the fragmented strength, which is, from a theoretical point of view, a result of the couplings involving complex configurations, e.g., of two-particle–two-hole (2p-2h) interactions as pointed out, for example, in Ref. [75]. However, introduction of 2p-2h effects is technically demanding task going beyond the scope of this work, and we leave it for the future study. In this work, we use the g factors of the bare nucleons; i.e., the quenching effect has not been considered.

The reduced matrix elements for the isoscalar or isovector component of the $M1$ operator in Eq. (9) are given by

$$\langle j_f||\hat{\boldsymbol{\mu}}^{(X)}||j_i\rangle = I_{\mathrm{large}}\langle(\tfrac{1}{2},\ell_f)j_f||\hat{\boldsymbol{\mu}}^{(X)}(11)||(\tfrac{1}{2},\ell_i)j_i\rangle + I_{\mathrm{small}}\langle(\tfrac{1}{2},\tilde{\ell}_f)j_f||\hat{\boldsymbol{\mu}}^{(X)}(22)||(\tfrac{1}{2},\tilde{\ell}_i)j_i\rangle, \quad (13)$$

where X = IS or IV, respectively. Here the radial parts of these matrix elements are given by the integrals

$$I_{\mathrm{large}} = \int_0^\infty f^*_{n_f j_f}(r) f_{n_i j_i}(r) r^2 dr \quad (14)$$

and

$$I_{\mathrm{small}} = \int_0^\infty g^*_{n_f j_f}(r) g_{n_i j_i}(r) r^2 dr, \quad (15)$$

where $f_{nj}(r)$ are large and $g_{nj}(r)$ small radial components of the quasiparticle Dirac spinors for nucleons [65]. The labels j_i and j_f denote total nucleon angular momenta of the initial and final states, respectively. The orbital angular momenta that correspond to large (l_i, l_f) and small $(\tilde{l}_f, \tilde{l}_i)$ spinor components are determined by the total angular momenta (j_i, j_f) and parity (π_i, π_f) of the initial and final states [65]. Thus, the $M1$ transition strength in the RQRPA formalism is given by

$$B(M1,E) = \left|\sum_{\kappa\kappa'}\left(X^{\nu,10}_{\kappa\kappa'} - (-1)^{j_\kappa - j_{\kappa'}}Y^{\nu,10}_{\kappa\kappa'}\right) \times (u_\kappa v_{\kappa'} - v_\kappa u_{\kappa'})\left\langle j_{\kappa'};\frac{1}{2}\,t_z||\hat{\boldsymbol{\mu}}||j_\kappa;\frac{1}{2}\,t_z\right\rangle\right|^2. \quad (16)$$

Similarly, following Eq. (8), the isovector transition strength reads

$$B^{(\mathrm{IV})}(M1,E) = \left|-\sum_{\kappa\kappa'}\frac{C_{M1}}{\sqrt{2t_f+1}}\left\langle\frac{1}{2}||\hat{\tilde{\tau}}||\frac{1}{2}\right\rangle \times\left[X^{\nu,10}_{\kappa\kappa'} - (-)^{j_\kappa - j_{\kappa'}}Y^{\nu,10}_{\kappa\kappa'}\right] \times (u_\kappa v_{\kappa'} - v_\kappa u_{\kappa'})\langle j_{\kappa'}||\hat{\boldsymbol{\mu}}^{(\mathrm{IV})}||j_\kappa\rangle\right|^2, \quad (17)$$

whereas the isoscalar strength is given by

$$B^{(\mathrm{IS})}(M1,E) = \left|\sum_{\kappa\kappa'}\left\langle\frac{1}{2}||1_\tau||\frac{1}{2}\right\rangle\left[X^{\nu,10}_{\kappa\kappa'} - (-)^{j_\kappa - j_{\kappa'}}Y^{\nu,10}_{\kappa\kappa'}\right] \times (u_\kappa v_{\kappa'} - v_\kappa u_{\kappa'})\langle j_{\kappa'}||\hat{\boldsymbol{\mu}}^{(\mathrm{IS})}||j_\kappa\rangle\right|^2. \quad (18)$$

In the following calculations, we also refer to the spin-$M1$ transition strength,

$$B^\sigma(M1,E) = B(M1,E)|_{g_\ell=0}, \quad (19)$$

where the orbital gyromagnetic factors are set to zero. Similarly, the orbital $M1$ strength is given as

$$B^\ell(M1,E) = B(M1,E)|_{g_s=0}. \quad (20)$$

For the analysis of $M1$ transition strength, energy-weighted moments m_k of the discrete spectra are used:

$$m_k = \sum_\nu B(MJ,\omega_\nu)(E_\nu - E_0)^k. \quad (21)$$

Two moments are often used in order to compare experimental results with theoretical predictions, i.e., the non-energy-weighted sum m_0, which corresponds to the total strength

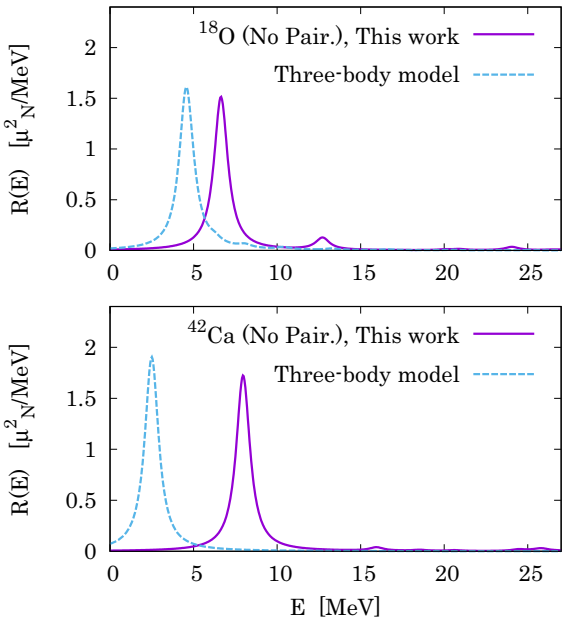

FIG. 1. (Top) The $M1$ transition strength distributions for ^{18}O (upper panel) and ^{42}Ca (lower panel) based on the RRPA calculations with DD-PC1 parametrization. The result from the three-body model without pairing from Ref. [29] is shown for comparison.

$B(M1)$, and energy-weighted sum of the strength m_1. A quotient of two moments, $\bar{E} = m_1/m_0$, corresponds to the centroid energy which represents an average energy of discrete strength distribution.

C. The $M1$ sum rule in core-plus-two-nucleon systems

For a consistency check of numerical calculations of nuclear excitations, such as giant resonances, the sum rules related to the transition strength have provided in the past useful guidance [76–81]. In this section, the $M1$ sum rule introduced in Ref. [29] is utilized to test the validity of the framework established in this work. In Ref. [29], the non-energy-weighted sum ($m_{k=0}$) of the $M1$ excitation was evaluated for some specific systems, which consist of the core with shell closure and two additional valence neutrons or protons, e.g., ^{18}O and ^{42}Ca. If the pairing correlations between the valence nucleons are neglected, one advantage of that sum rule is that its non-energy-weighted sum-rule value (SRV) is determined analytically for the corresponding system of interest.

In this section, we perform the calculation of the $M1$ SRV within the relativistic random phase approximation (RRPA), based on the formalism given in Sec. II. The DD-PC1 functional is used, supplemented with the IV-PV channel in the RRPA residual interaction, with the strength parameter $\alpha_{\text{IV-PV}} = 0.53$ fm^2, in the natural system of units. Note that in this sum rule test, the pairing correlations are neglected in calculations. Figure 1 displays the $M1$-response function $R(E)$ from Eq. (6) for ^{18}O and ^{42}Ca, obtained with the RRPA. Our result shows the dominant single peak in each system. Table I shows the non-energy-weighted sum (m_0) results for $M1$ transitions in ^{18}O and ^{42}Ca obtained from the RRPA. The

TABLE I. Non-energy-weighted sum ($m_{k=0}$) of the $M1$ response function for ^{18}O and ^{42}Ca obtained from the RRPA calculation. The analytical SRV value from Ref. [29] is shown for comparison. The unit is μ^2_N.

	m_0 (This work)	SRV [29]
^{18}O	2.73	2.79
^{42}Ca	2.91	2.99

m_0 value is calculated from Eq. (21), using the $M1$ strength distribution up to 50 MeV. For comparison, the respective values introduced in Ref. [29] are also shown as "SRV." The RRPA accurately reproduces the SRVs for the two nuclei under consideration. Namely, the relativistic framework to describe the $M1$ transitions appears to be valid at the level of no-pairing limit. The small deficiency of RRPA beyond the SRV value is attributable to the cutoff energy.

As shown in Fig. 1, the RRPA excitation energy of the $M1$ mode appears different than in the case of three-body model from Ref. [29]. This discrepancy originates from different open shell structures produced by the two models. For further improvement, one may adjust these models directly to the $M1$-reference data, which have been, however, not precisely obtained for ^{18}O or ^{42}Ca. Nevertheless, since the sum rule does not depend on the excitation energy, the analysis of both approaches confirms the expected $M1$-sum values and thus justifies our RRPA implementation.

III. RESULTS

In the following, we present the results of $M1$ transitions based on the RHB+R(Q)RPA framework introduced in Sec. II. The functional DD-PC1 [65] is systematically used in model calculations, supplemented with the pairing interaction from the phenomenological Gogny-D1S force [69].

A. $M1$ transitions in ^{208}Pb

As the first case for detailed analysis of $M1$ transitions in the framework based on the RNEDF, we the consider ^{208}Pb nucleus. There is experimental data on this system available [37–39,41–43], and thus, it is suitable for the first application. Figure 2 shows the $M1$ response function $R_{M1}(E)$ for ^{208}Pb, obtained using Eq. (6). Since it is a magic nucleus, pairing correlations do not contribute to the nuclear ground-state energy, and the RHB + RQRPA reduces to the relativistic Hartree + RRPA model. In addition to the full response $R_{M1}(E)$, the responses to the isoscalar and isovector operators, $R^{\text{IS}}_{M1}(E)$ and $R^{\text{IV}}_{M1}(E)$, are shown separately. For comparison, the so-called "unperturbed" response at the Hartree level is also shown, corresponding to the limit when the residual RRPA interaction is set to zero.

As shown in Fig. 2, the full $M1$ response is dominated by the two peaks at 6.11 and 7.51 MeV. These two peaks exhaust most of the total $M1$ strength up to 50-MeV energy. In some experimental studies [37,38], a dominant peak of the $M1$ strength distribution around 7.0–7.5 MeV has been measured, whereas the other bump could be found at ≈6.2 MeV [38].

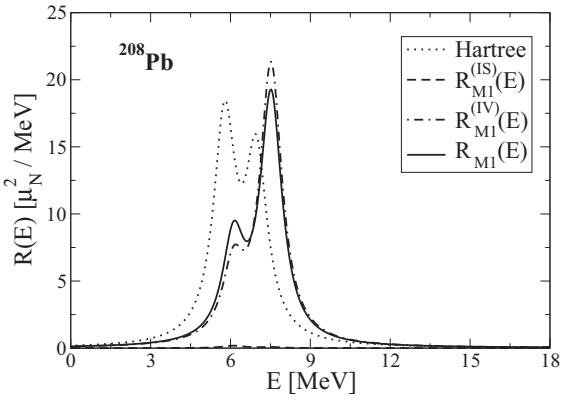

FIG. 2. The $M1$ transition strength distribution for ^{208}Pb. The results are obtained with the RRPA using the DD-PC1 functional: $R_{M1}(E)$ for full, $R^{(\mathrm{IS})}_{M1}(E)$ for isoscalar, and $R^{(\mathrm{IV})}_{M1}(E)$ for isovector response functions. Unperturbed response at the Hartree level is also shown.

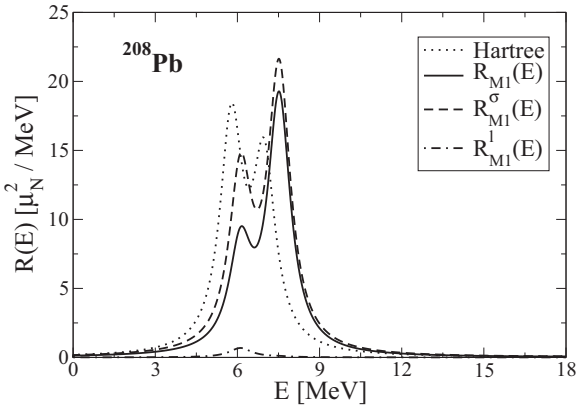

FIG. 3. The same as Fig. 2, but with $R(M1)$ full, $R^{\sigma}_{M1}(E)$ spin, and $R^{\ell}_{M1}(E)$ orbital response functions. Unperturbed response at the Hartree level is also shown.

However, the experimental data also show a more fine fragmentation of the $M1$ strength in ^{208}Pb [37,38]. To reproduce this fragmentation, the present RRPA may need to be improved with, e.g., the two-particle–two-hole effect [75], which is beyond the present scope. Even with the lack of detail, our RRPA scheme reproduces the rough structure of the $M1$ distribution of ^{208}Pb, especially its dominant two-peak structure. By comparing the full $M1$ response with the unperturbed response at the Hartree level (Fig. 2), one can observe that the full response is shifted to higher energies, demonstrating the effect of the IV-PV residual interaction to establish $M1$ transitions as a genuine nuclear mode of excitation. This shift is consistent to the selection rule of $M1$, since the IV-PV interaction affects the $J^{\pi} = 1^{+}$ excited states.

In Fig. 2, one can observe that the isovector $M1$ response is significantly larger than the isoscalar one, and both components interfere. The dominance of isovector mode is visible also from the $M1$ strength integrated up to 50 MeV: The full strength amounts $\sum B(M1) = 41.99\ \mu_N^2$, whereas the isoscalar strength is $\sum B^{(\mathrm{IS})}(M1) = 0.43\ \mu_N^2$ and the isovector strength is $\sum B^{(\mathrm{IV})}(M1) = 42.33\ \mu_N^2$. The main reason of the isovector $M1$ dominance is a large difference in the respective gyromagnetic ratios, g_s^{IS} and g_s^{IV} given in Eqs. (11) and (12). For more details, see the Appendix.

The structure of the two pronounced $M1$ peaks is analyzed in more detail. Table II shows the respective partial contributions b_{ph} to the B(M1) strength from the major proton and neutron particle-hole (ph) configurations [see Eq. (7)]. That is, if single proton ($\mathrm{p_1h_1}$) and neutron ($\mathrm{p_2h_2}$) configurations contribute to the $M1$ transition at excitation energy E,

$$B(M1,\ E) = \left|b^{\nu}_{\mathrm{p_1h_1}}(E) + b^{\pi}_{\mathrm{p_2h_2}}(E)\right|^2. \tag{22}$$

For the state at 6.11 MeV, the major contribution comes from the transitions between spin-orbit partner states for neutrons ($\nu 1i^{-1}_{13/2} \rightarrow \nu 1i_{11/2}$) and protons ($\pi 1h^{-1}_{11/2} \rightarrow \pi 1h_{9/2}$). As shown in Table II, partial proton and partial neutron spin-flip transitions interfere destructively. In the case of the state at 7.51 MeV, the main transitions are ($\nu 1i^{-1}_{13/2} \rightarrow \nu 1i_{11/2}$) and ($\pi 1h^{-1}_{11/2} \rightarrow \pi 1h_{9/2}$), with coherent contributions to the total $B(M1)$ strength, as shown in Table II.

Figure 3 shows the separation of the full $M1$ response in ^{208}Pb to the spin and orbital response functions, $R^{\sigma}_{M1}(E)$ and $R^{\ell}_{M1}(E)$, evaluated by Eqs. (19) and (20), respectively. One can observe considerably larger spin response in comparison to the orbital one; i.e., most of the overall $B(M1)$ strength is exhausted by the spin $M1$ response. The orbital $M1$ strength is mainly related to deformation and almost disappears in the closed-shell nuclei [3]. The spin and orbital responses interfere destructively, i.e., the full response function is smaller than the spin response. The corresponding sums of the strengths amount to $53.14\ \mu_N^2$ for the spin, $1.19\ \mu_N^2$ for the orbital, and $41.99\ \mu_N^2$ for the full $M1$ transition. In the present study of ^{208}Pb, the overall $M1$ excitation strength is almost fully exhausted by the two peaks, i.e., $B(M1, E = 6.11\ \mathrm{MeV}) = 11.6\ \mu_N^2$ and $B(M1, E = 7.51\ \mathrm{MeV}) = 28.96\ \mu_N^2$.

Over the past years, there have been several experimental studies of $M1$ transitions in ^{208}Pb. Several experimental results are summarized in a chronological order in Table III. It turns out that the total measured strength lies between $\sum B(M1) \cong (35.0\text{–}47.5)\ \mu_N^2$ and it is in agreement with our result. However, from recent experiments [37–39], it has also been pointed out that the actual $M1$ sum could need to be reduced, mainly due to the confusion with the electric-dipole components in the old experiments. A recent theoretical investigation based on the Skyrme functional [18] results even in lower $B(M1)$ strength in comparison to the modern experiments. Therefore, quantitative description of the

TABLE II. Partial neutron and proton contributions ($b^{\nu,\pi}_{\mathrm{ph}}$) to the $M1$ transition strength for the two main peaks (E_{peak}), and respective overall transition strengths $B(M1)$ for ^{208}Pb. Details about configurations are given in the text.

$E^{\mathrm{th.}}_{\mathrm{peak}}$ [MeV]	b^{ν}_{ph} [μ_N]	b^{π}_{ph} [μ_N]	$B(M1)$ [μ_N^2]
6.11	−1.33	4.74	11.6
7.51	4.22	1.15	28.96

TABLE III. A summary of reported experimental $M1$ excitation energies and transition strengths in ^{208}Pb. In Ref. [42], the symbol (*) denotes experimental ambiguity due to parity assignment to the quantum mechanical state with respect to $M1$ transitions.

(^{208}Pb)	E_x [MeV]	$B_{M1,\uparrow}$ [μ_N^2]
Ref. [43] (1977)	(sum)	35.0
Ref. [41] (1977)	(sum)	46.5
Ref. [42] (1979)	4.843	5.8*
	7.061	17.7*
	7.249	0.5
	7.37–7.82	7.9
	7.98	7.1*
	8.20–9.50	8.5
	4.843–9.50	$\sum B(M1,E)_\uparrow$ = 47.5 (30.6*)
Ref. [39] (1985)	5.8–7.4	10.7
	⩽6.4	1.9
	7.3	15.6
Ref. [38] (1988)	6.7–8.1	19.0
Ref. [37] (2016)	7.0–9.0	20.5

transition strengths for $M1$ modes remains an open question. In comparison to Bohr and Mottelson's independent particle model (IPM), which estimates $B(M1) = 36\ \mu_N^2$ in Ref. [40], the RRPA result is comparable but somewhat higher. In Refs. [16–18], the similar calculation based on the Skyrme functionals have been used, with the quenching factors in g coefficients, $\simeq$0.65, in order to reduce the transition strength. When using the quenching, the total $B(M1)$ strength for ^{208}Pb obtained for a set of Skyrme parametrizations amounts 14.8–17.3 μ_N^2 [16].

B. $M1$ transitions in ^{48}Ca

In the following, we extend our study to the lighter system, the ^{48}Ca nucleus, where several experimental data are available [37,82,83]. In Fig. 4, the RRPA full, isoscalar, and isovector $B(M1)$ transition-strength distributions are shown for ^{48}Ca. The $M1$ strength distribution is composed from a single dominant peak. The corresponding transition strength

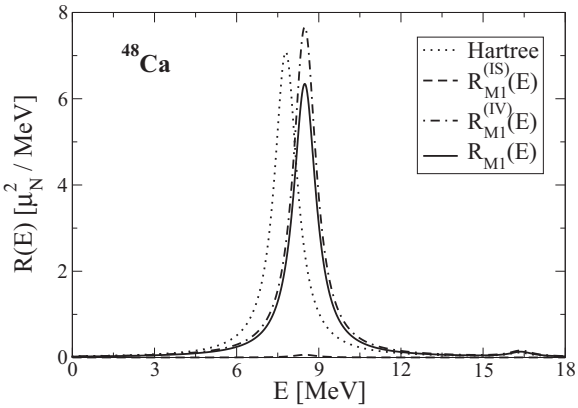

FIG. 4. The same as Fig. 2, but for ^{48}Ca.

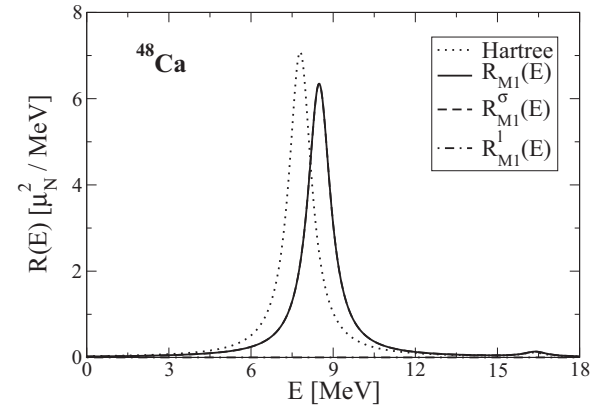

FIG. 5. The same as Fig. 3 but for ^{48}Ca. The spin and full response functions coincide.

summed up to 50 MeV amounts to $B(M1) = 10.38\ \mu_N^2$ (total), $B^{(\mathrm{IS})}(M1) = 0.11\ \mu_N^2$, and $B^{(\mathrm{IV})}(M1) = 12.52\ \mu_N^2$. As in the case of ^{208}Pb, the isovector strength is larger than the isoscalar one. The centroid and peak energies of the full response are $\bar{E}^{\mathrm{th.}} = 9.37$ MeV and $E^{\mathrm{th.}}_{\mathrm{peak}} = 8.48$ MeV, respectively. On the other side, in the experimental investigation of $M1$ spin-flip resonance from inelastic proton scattering on ^{48}Ca [37], the dominant peak locates at slightly higher energy, $E^{\mathrm{exp.}}_{\mathrm{peak}} = 10.22$ MeV. We note that the present IV-PV interaction, which controls the $M1$ excited state of the 1^+ configuration, is described with the simple, constant coupling. By comparing the full response with the unperturbed one, the RRPA residual interaction shifts the main peak toward higher energy (Fig. 4). This is similar to the ^{208}Pb case, demonstrating the effect of the residual RRPA interaction.

Figure 5 shows the full, spin, and orbital $M1$ transition strength distributions for ^{48}Ca. The corresponding $B(M1)$ values are 10.38 μ_N^2, 10.40 μ_N^2, and $5.35 \times 10^{-3}\ \mu_N^2$, respectively. As in the case of heavy system ^{208}Pb, the spin transition strength dominates; i.e., it is four orders of magnitude larger than the orbital strength, $B^{\sigma}(M1) \gg B^{\ell}(M1)$.

From the analysis of the major $M1$ state at 8.48 MeV, we confirmed that it is composed mainly from the transition between the neutron spin-orbit partner states, $(\nu 1f_{7/2}^{-1} \rightarrow \nu 1f_{5/2})$. The major partial neutron and proton contributions to the $B(M1)$ strength are presented in Table IV, showing the dominance of the neutron spin-flip transitions over the proton ones.

In the experimental investigation of $M1$ spin-flip resonance from inelastic proton scattering on ^{48}Ca [37], the dominant peak at $E^{\mathrm{exp.}}_{\mathrm{peak}} = 10.22$ MeV is of pure neutron character, dominated by the transition $(\nu 1f_{7/2}^{-1} \rightarrow \nu 1f_{5/2})$. This character is

TABLE IV. Partial neutron and proton contributions ($b^{\nu,\pi}_{\mathrm{ph}}$) to the $M1$ transition strength and the full transition strength $B(M1)$ for the major peak at 8.48 MeV for ^{48}Ca.

$E^{\mathrm{th.}}_{\mathrm{peak}}$ [MeV]	b^{ν}_{ph} [μ_N]	b^{π}_{ph} [μ_N]	$B(M1)$ [μ_N^2]
8.48	3.18	4.04×10^{-4}	9.96

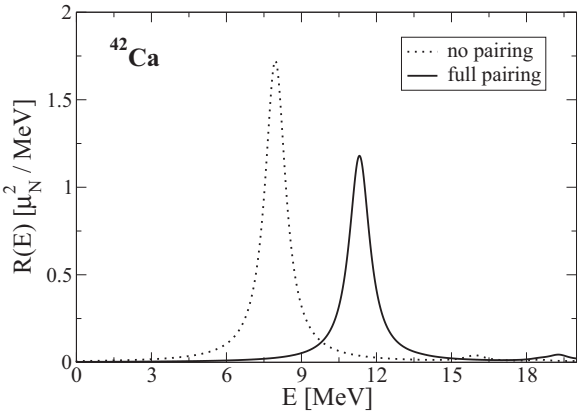

FIG. 6. The RHB + RQRPA response for $M1$ transitions in ^{42}Ca using the DD-PC1 parametrization and Gogny pairing correlations. The response functions without pairing correlations (RRPA) and with full pairing (RQRPA) are shown separately.

consistent with results obtained in the present study. The measured strength is obtained as $\sum B(M1) = 3.85$–$4.63\ \mu_N^2$ [37]. In Ref. [37], the data on ^{48}Ca(p, n) reaction [82] have also been reanalyzed, resulting with $\sum B(M1) = 3.45$–$4.10\ \mu_N^2$. Comparison with the RRPA results from the present analysis, $\sum B(M1) = 10.38\ \mu_N^2$, indicates the enhancement of the theoretical prediction for the $B(M1)$ transition strength. We note that another experimental study, based on the (γ, n) reaction [83], resulted in a value twice as large as that in (p, p') reaction [37], $B(M1) = 6.8 \pm 0.5\ \mu_N^2$. This measurement is closer, but still below the result of our present work. One possibility to remove this discrepancy is by introducing the quenching factor $\eta \simeq 0.6$–0.7 for the $g_{s,\ell}$ coefficients. In this case, our sum of the $B(M1)$ strength changes as $\sum B(M1) \longrightarrow \eta^2 \sum B(M1) \simeq 3.7$–$5.1\ \mu_N^2$. Note that the similar quenching factors have been utilized in several theoretical calculations [16,17]. For example, a study based on Skyrme functionals results in $B(M1)$ values 2.5–4.8 μ_N^2 [16].

C. Pairing effects on $M1$ transitions

In this section, we apply the complete RHB + RQRPA framework adopted for the description of $M1$ transitions in open-shell nuclei, by consistent implementation of the pairing correlations in the nuclear ground state and in the RQRPA residual interaction. The main purpose here is to explore the role of the pairing correlations on the properties of the $M1$ response. The sensitivity of the $M1$ transitions on pairing correlations has previously been addressed in the study based on the three-body model [29]. In the present study, we discuss the same aspect but utilize a microscopic RNEDF approach.

As the first open-shell system, we study ^{42}Ca, which is already considered in its no-pairing limit in Sec. II C in order to verify the $M1$ sum rule in the core-plus-two-nucleon system [29]. In Fig. 6, the results of the full RHB + RQRPA calculation are shown, in comparison to the limit without pairing correlations both in the ground state (GS) and in the residual interaction. The full-RQRPA $M1$ response shows one major peak at 11.32 MeV that is composed mainly by a single-neutron $2qp$ transition, $(\nu 1f_{7/2}^{-1} \rightarrow \nu 1f_{5/2})$. In comparison to the peak obtained in RRPA calculation without pairing correlations, the pairing interaction shifts the resonant peak by several MeV to higher energies and reduces its strength. This shift by the pairing correlations at the quantitative level can also be seen in Table V. The present result is consistent with that in Ref. [29]: The pairing interaction, which promotes the spin-singlet pairing between the valence nucleons, shifts the $M1$ excitation energy toward higher region, with a reduction of the strength, $B(M1)$. We note that the pairing effect in the particle-particle channel of the residual RQRPA interaction is finite but very small for the $M1$ transition from the 0^+ GS to 1^+ excited states. The major pairing effects originate from the properties of the GS. The same effect has been theoretically observed for the surface δ interaction applied on the $M1$ excitations in the particle-particle channel [84].

TABLE V. The peak energies $E_{\text{peak}}^{\text{th.}}$ and corresponding $B(M1)$ values for ^{42}Ca and ^{50}Ti in this work.

Nuclides	Method	$E_{\text{peak}}^{\text{th.}}$ [MeV]	$B(M1)$ [μ_N^2]
^{42}Ca	RRPA	7.95	2.92
	RQRPA	11.32	2.12
^{50}Ti	RRPA	8.82	13.86
	RQRPA	8.58	8.53
		11.57	3.88

Next we move to the ^{50}Ti nucleus, where the $M1$ excitations from its GS have been measured [85]. These data can be utilized as reference to infer the present accuracy and drawback of the RQRPA calculations. In Fig. 7, our result is presented in the case of calculations with and without pairing correlations. The respective properties of $M1$ transitions are tabulated in Table V. In the ^{50}Ti case, the pairing interaction causes the main peak to split into two: $E_{\text{peak}}^{\text{th.}} = 8.58$ and 11.57 MeV. This two-peak structure has been confirmed in the experiments at $E_{\text{peak}}^{\text{exp.}} \cong 8.7$ and 10.2 MeV [85]. Thus, the RQRPA reasonably reproduces the general structure of $M1$ excitation spectrum. Considering the deviation of calculated energies from the empirical values, further development and/or optimization of the RNEDF is required. Note also that,

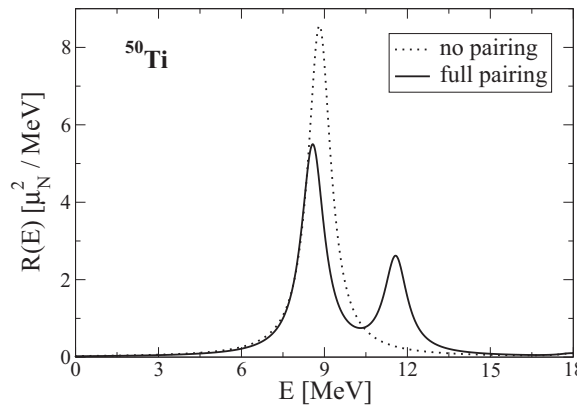

FIG. 7. The same as Fig. 6 but for ^{50}Ti.

as we discussed in the previous sections, the actual data from experiments suggests a finer fragmentation, for which complicated additional effects may need to be considered, e.g., the meson-exchange current effect [3,22,26,49,50,86] and/or the second-order (Q)RPA [75,87,88].

The RQRPA calculations show that the two main $M1$ peaks in ^{50}Ti mainly originate from the proton transition of $(\pi 1f_{7/2}^{-1} \rightarrow \pi 1f_{5/2})$ and neutron transition of $(\nu 1f_{7/2}^{-1} \rightarrow \nu 1f_{5/2})$. This is because of the shell closure at $Z = N = 20$, and thus the main $M1$ excitation components are attributed to the valence, two protons, and eight neutrons in the $1f_{7/2}$ orbit.

IV. SUMMARY

In this work, we have introduced an approach to describe $M1$ transitions in nuclei, based on the RHB + RQRPA framework with the relativistic point-coupling interaction, supplemented with the pairing correlations described by the pairing part of the Gogny force. In addition to the standard terms of the point coupling model with the DD-PC1 parametrization, the residual R(Q)RPA interaction has been extended by the isovector-pseudovector contact type of interaction that contributes to unnatural parity transitions. A recently developed nonpairing $M1$ sum rule in core-plus-two-nucleon systems [29] has been used as a consistency check of the present theory framework. The sum of the $M1$ transition strength for ^{42}Ca accurately reproduced the sum rule value (SRV), thus validating the introduced formalism and its numerical implementation for further exploration of $M1$ transitions.

The present framework is first benchmarked on $M1$ transitions for two magic nuclei, ^{48}Ca and ^{208}Pb. The response functions $B(M1, E)$ have been explored in detail, including their isoscalar and isovector components, that relate to the electromagnetic probe, as well as contributions of the spin and orbital components of the $M1$ transition operator. It is confirmed that, in nuclei without deformation, the spin component of the $M1$ transition strength dominates over the orbital one. Because of the differences in the gyromagnetic ratios, the isovector $M1$ transition strength is significantly larger than the isoscalar one, and they interfere destructively. It is shown that the major peaks of isovector spin-$M1$ transitions are dominated mainly by a single ph configuration composed of spin-orbit partner states.

One of our interests was to investigate the role of the pairing correlations on the properties of $M1$ response functions in open shell nuclei, which has been addressed in the study of ^{42}Ca and ^{50}Ti. The RQRPA calculations show a significant impact of pairing correlations on the major peak by shifting it to the higher energies and, at the same time, by reducing the transition strength. In the ^{50}Ti case, this effect is essential to reproduce the two-peak structure measured in the experiment [85]. The main effect of the pairing correlations is observed at the level of the ground-state calculation, while it is rather small in the particle-particle channel of the residual RQRPA interaction.

The $M1$ transition strengths from the present study appear larger than the values obtained from the experimental data. Therefore, it remains an open question whether some additional effects should be included at the theory side, or some strength may be missing in the experimental data. In addition, the $M1$ excitation energies of light systems, e.g., ^{48}Ca, still have some deviation from the reference data. In order to resolve these open questions, further developments are needed, e.g., resolving the quenching effects in g factors, meson exchange effects, couplings with complex configurations, etc. Because of its relation to the spin-orbit interaction, $M1$ excitations could also provide guidance toward more advanced RNEDFs. Recently, a new relativistic energy density functional has been constrained not only by the ground-state properties of nuclei, but also by using the $E1$ excitation properties (i.e., dipole polarizability) and giant monopole resonance energy in ^{208}Pb [66]. Similarly, $M1$ excitation properties in selected nuclei could also be exploited in the future studies to improve the RNEDFs.

ACKNOWLEDGMENTS

This work is supported by the "QuantiXLie Centre of Excellence," a project cofinanced by the Croatian Government and European Union through the European Regional Development Fund, the Competitiveness and Cohesion Operational Programme (KK.01.1.1.01).

APPENDIX: ISOSCALAR-ISOVECTOR (IS-IV) DECOMPOSITION

In this Appendix, we give some details on the IS-IV decomposition of the transition operator in a general consideration that applies both to electric and magnetic transitions. Namely, we consider the $X\lambda\mu$ transition, where X denotes E or M for electric and magnetic transitions, respectively, and $(\lambda, \ -\lambda < \mu < \lambda)$ denote the multipole quantum numbers. The A-body operator of the $X\lambda\mu$ transition is given as

$$\hat{\mathcal{P}}(X\lambda\mu) = \sum_{i=1}^{A} \hat{\mathcal{Q}}(X\lambda\mu; i), \tag{A1}$$

where $\hat{\mathcal{Q}}$ is the general single-particle operator. Then, by using the isospin $\tau_3 = +1$ (-1) for protons (neutrons), it is expressed as

$$\begin{aligned}\hat{\mathcal{P}}(X\lambda\mu) &= \sum_{k\in Z} f_{X\lambda}^{\pi} \hat{\mathcal{S}}(X\lambda\mu; \boldsymbol{r}_k) + \sum_{l\in N} f_{X\lambda}^{\nu} \hat{\mathcal{S}}(X\lambda\mu; \boldsymbol{r}_l), \\ &= \sum_{i=1}^{A} \left[f_{X\lambda}^{\pi} \frac{1+\hat{\tau}_3(i)}{2} + f_{X\lambda}^{\nu} \frac{1-\hat{\tau}_3(i)}{2} \right] \\ &\quad \times \hat{\mathcal{S}}(X\lambda\mu; \boldsymbol{r}_i),\end{aligned} \tag{A2}$$

where $f_{X\lambda}^{\pi\,(\nu)}$ indicates the charge (for $E\lambda$) or gyromagnetic factor (for $M\lambda$) of the $X\lambda$ mode for protons (neutrons) and $\hat{\mathcal{S}}(X\lambda\mu; \boldsymbol{r}_i)$ is the transition operator. See Table VI for some examples of $E2$ and $M1$ transitions [81].

From Eq. (A2), the IS-IV decomposition is derived:

$$\begin{aligned}\hat{\mathcal{P}}(X\lambda\mu) &= \hat{\mathcal{P}}^{\mathrm{IS}}(X\lambda\mu) + \hat{\mathcal{P}}^{\mathrm{IV}}(X\lambda\mu) \\ &= f_{X\lambda}^{\mathrm{IS}} \sum_{i=1}^{A} \hat{\mathcal{S}}(X\lambda\mu; \boldsymbol{r}_i) + f_{X\lambda}^{\mathrm{IV}} \sum_{i=1}^{A} \hat{\mathcal{S}}(X\lambda\mu; \boldsymbol{r}_i)\hat{\tau}_3(i).\end{aligned} \tag{A3}$$

TABLE VI. The transition operators and respective proportionality factors for $E2$ and $M1$ (orbital and spin part) modes [81]. See text for details.

$X\lambda$	$(f^\pi,\ f^\nu)$	$(f^{\rm IS},\ f^{\rm IV})$	$\hat{\mathcal{S}}(\boldsymbol{r})$
$E2$	$(e,\ 0)$	$(e/2,\ e/2)$	$r^2 Y_{2\mu}(\hat{\boldsymbol{r}})$
$M1,\ l$	$(g_l^\pi,\ g_l^\nu)$	$(g_l^{\rm IS},\ g_l^{\rm IV})$	$\mu_{\rm N}(\hat{\boldsymbol{l}}\cdot\boldsymbol{r}/r)_\mu$
	$=(1,\ 0)$	$=(1/2,\ 1/2)$	$\times\sqrt{3/4\pi}$
$M1,\ s$	$(g_s^\pi,\ g_s^\nu)$	$(g_s^{\rm IS},\ g_s^{\rm IV})$	$\mu_{\rm N}(\hat{\boldsymbol{s}}\cdot\boldsymbol{r}/r)_\mu$
	$=(5.586,\ -3.826)$	$=(0.880,\ 4.706)$	$\times\sqrt{3/4\pi}$

Omitting the subscript $X\lambda$ for simplicity, the $f^{\rm IS}$ and $f^{\rm IV}$ factors are determined as

$$f^{\rm IS}=\frac{f^\pi+f^\nu}{2},\quad f^{\rm IV}=\frac{f^\pi-f^\nu}{2}, \tag{A4}$$

and equivalently, $f^\pi=f^{\rm IS}+f^{\rm IV}$ and $f^\nu=f^{\rm IS}-f^{\rm IV}$. It is useful to check the relation between the proton-neutron and IS-IV decompositions. That is, by using $\hat{\mathcal{X}}^\pi=\sum_{k\in Z}\hat{\mathcal{S}}(X\lambda\mu;k)$ and $\hat{\mathcal{X}}^\nu=\sum_{l\in N}\hat{\mathcal{S}}(X\lambda\mu;l)$,

$$\begin{aligned}\hat{\mathcal{P}}^{\rm IS}(X\lambda\mu)&=f^{\rm IS}[\hat{\mathcal{X}}^\pi+\hat{\mathcal{X}}^\nu],\\ \hat{\mathcal{P}}^{\rm IV}(X\lambda\mu)&=f^{\rm IV}[\hat{\mathcal{X}}^\pi-\hat{\mathcal{X}}^\nu],\end{aligned} \tag{A5}$$

where we have implemented $\tau_3=-1$ for neutrons in the last term. Then, it is worthwhile to consider some special cases as follows.

First, we assume that only the neutron component is active for the transition, namely, $\langle f\,|\,\hat{\mathcal{X}}^\pi\,|\,i\rangle\cong 0$ and $\langle f\,|\,\hat{\mathcal{X}}^\nu\,|\,i\rangle\neq 0$, like as the ^{48}Ca result in the main text. In this case, if $f^{\rm IS}\ll f^{\rm IV}$, likely as spin $M1$, the corresponding IV mode becomes dominant. That is,

$$\begin{aligned}|\langle f\,|\,\hat{\mathcal{P}}^{\rm IS}\,|\,i\rangle|^2&\ll|\langle f\,|\,\hat{\mathcal{P}}^{\rm IV}\,|\,i\rangle|^2\\ &\cong|f^{\rm IV}|^2|\langle f\,|\,\hat{\mathcal{X}}^\nu\,|\,i\rangle|^2.\end{aligned} \tag{A6}$$

Otherwise, if $f^{\rm IS}\cong f^{\rm IV}$ likely as $E2$ and orbit $M1$,

$$|\langle f\,|\,\hat{\mathcal{P}}^{\rm IS}\,|\,i\rangle|^2\cong|\langle f\,|\,\hat{\mathcal{P}}^{\rm IV}\,|\,i\rangle|^2. \tag{A7}$$

Note also that, by considering the IS+IV response,

$$\begin{aligned}\langle f\,|\,\hat{\mathcal{P}}^{\rm IS}+\hat{\mathcal{P}}^{\rm IV}\,|\,i\rangle&=f^\pi\langle f\,|\,\hat{\mathcal{X}}^\pi\,|\,i\rangle+f^\nu\langle f\,|\,\hat{\mathcal{X}}^\nu\,|\,i\rangle\\ &\cong 0+f^\nu\langle f\,|\,\hat{\mathcal{X}}^\nu\,|\,i\rangle,\end{aligned} \tag{A8}$$

then, this response vanishes when $f^\nu=0$, as in the $E2$ and orbit $M1$ cases. In Fig. 5 for ^{48}Ca, indeed the orbit $M1$ response is zero, and the total and spin $M1$ results coincide.

Next, when the proton and neutron excitations occur in the same phase, it means

$$\langle f\,|\,\hat{\mathcal{X}}^\nu\,|\,i\rangle\propto(+)\langle f\,|\,\hat{\mathcal{X}}^\pi\,|\,i\rangle, \tag{A9}$$

and thus,

$$|\langle f\,|\,\hat{\mathcal{X}}^\pi-\hat{\mathcal{X}}^\nu\,|\,i\rangle|^2\ll|\langle f\,|\,\hat{\mathcal{X}}^\pi+\hat{\mathcal{X}}^\nu\,|\,i\rangle|^2. \tag{A10}$$

In this case, as long as $f^{\rm IS}\cong f^{\rm IV}$, the IS mode is obviously dominant. Otherwise, the result can depend on the competition of the $f^{\rm IS}/f^{\rm IV}$ ratio against the weightless amplitudes in Eq. (A10). Note also that, for this problem, the quantities $\langle f\,|\,\hat{\mathcal{X}}^\pi\,|\,i\rangle$ and $\langle f\,|\,\hat{\mathcal{X}}^\nu\,|\,i\rangle$ noticeably depend on the number of protons and neutrons, as well as the specific form of the transition operator. In our results in the main text, for the spin $M1$ mode, the IV component is concluded as dominant commonly for the nuclides discussed. This result is mainly attributed to that the factor $f^{\rm IV}=g_s^{\rm IV}$ is sufficiently larger than $f^{\rm IS}=g_s^{\rm IS}$.

Finally, when the proton and neutron excitations occur in the opposite phase, $\langle f\,|\,\hat{\mathcal{X}}^\nu\,|\,i\rangle\propto(-)\langle f\,|\,\hat{\mathcal{X}}^\pi\,|\,i\rangle$, and thus

$$|\langle f\,|\,\hat{\mathcal{X}}^\pi-\hat{\mathcal{X}}^\nu\,|\,i\rangle|^2\gg|\langle f\,|\,\hat{\mathcal{X}}^\pi+\hat{\mathcal{X}}^\nu\,|\,i\rangle|^2. \tag{A11}$$

In this case, the IV transition becomes dominant in the $E2$, orbit $M1$, and spin $M1$ cases, anyway.

[1] A. Richter, Prog. Part. Nucl. Phys. **13**, 1 (1985).
[2] A. Richter, Prog. Part. Nucl. Phys. **34**, 261 (1995).
[3] K. Heyde, P. von Neumann-Cosel, and A. Richter, Rev. Mod. Phys. **82**, 2365 (2010).
[4] U. Kneissl, H. Pitz, and A. Zilges, Prog. Part. Nucl. Phys. **37**, 349 (1996).
[5] N. Pietralla, P. von Brentano, and A. Lisetskiy, Prog. Part. Nucl. Phys. **60**, 225 (2008).
[6] T. Shizuma, T. Hayakawa, H. Ohgaki, H. Toyokawa, T. Komatsubara, N. Kikuzawa, A. Tamii, and H. Nakada, Phys. Rev. C **78**, 061303(R) (2008).
[7] S. Goriely, Nucl. Phys. A **933**, 68 (2015).
[8] S. Goriely, S. Hilaire, S. Péru, M. Martini, I. Deloncle, and F. Lechaftois, Phys. Rev. C **94**, 044306 (2016).
[9] K. Langanke, G. Martínez-Pinedo, P. von Neumann-Cosel, and A. Richter, Phys. Rev. Lett. **93**, 202501 (2004), and references therein.
[10] K. Langanke and G. Martínez-Pinedo, Rev. Mod. Phys. **75**, 819 (2003).
[11] K. Langanke, G. Martínez-Pinedo, B. Müller, H.-T. Janka, A. Marek, W. R. Hix, A. Juodagalvis, and J. M. Sampaio, Phys. Rev. Lett. **100**, 011101 (2008).
[12] H. P. Loens, K. Langanke, G. Martinez-Pinedo, and K. Sieja, Eur. Phys. J. A **48**, 34 (2012).
[13] M. B. Chadwick, M. Herman, P. Obložinský, M. E. Dunn, Y. Danon, A. C. Kahler, D. L. Smith, B. Pritychenko, G. Arbanas, R. Arcilla *et al.*, Nucl. Data Sheets **112**, 2887 (2011).
[14] T. Otsuka, T. Suzuki, R. Fujimoto, H. Grawe, and Y. Akaishi, Phys. Rev. Lett. **95**, 232502 (2005).
[15] T. Otsuka, T. Suzuki, M. Honma, Y. Utsuno, N. Tsunoda, K. Tsukiyama, and M. Hjorth-Jensen, Phys. Rev. Lett. **104**, 012501 (2010).
[16] P. Vesely, J. Kvasil, V. O. Nesterenko, W. Kleinig, P. G. Reinhard, and V. Y. Ponomarev, Phys. Rev. C **80**, 031302(R) (2009).
[17] V. O. Nesterenko, J. Kvasil, P. Vesely, W. Kleinig, P.-G. Reinhard, and V. Y. Ponomarev, J. Phys. G: Nucl. Part. Phys. **37**, 064034 (2010).
[18] V. Tselyaev, N. Lyutorovich, J. Speth, P.-G. Reinhard, and D. Smirnov, Phys. Rev. C **99**, 064329 (2019).
[19] J. D. Vergados, H. Ejiri, and F. Šimkovic, Rep. Prog. Phys. **75**, 106301 (2012).
[20] D. P. Arteaga and P. Ring, Phys. Rev. C **77**, 034317 (2008).

[21] J.-P. Ebran, E. Khan, D. Peña Arteaga, and D. Vretenar, Phys. Rev. C **83**, 064323 (2011).
[22] A. Richter, Nucl. Phys. A **507**, 99 (1990).
[23] T. Otsuka, Nucl. Phys. A **507**, 129 (1990).
[24] D. Bohle, A. Richter, W. Steffen, A. Dieperink, N. L. Iudice, F. Palumbo, and O. Scholten, Phys. Lett. B **137**, 27 (1984).
[25] D. Bohle, G. Küchler, A. Richter, and W. Steffen, Phys. Lett. B **148**, 260 (1984).
[26] R. Schwengner, S. Frauendorf, and B. A. Brown, Phys. Rev. Lett. **118**, 092502 (2017).
[27] E. B. Balbutsev, I. V. Molodtsova, and P. Schuck, Phys. Rev. C **97**, 044316 (2018).
[28] A. Repko, J. Kvasil, and V. O. Nesterenko, Phys. Rev. C **99**, 044307 (2019).
[29] T. Oishi and N. Paar, Phys. Rev. C **100**, 024308 (2019).
[30] N. D. Dang and N. Q. Hung, J. Phys. G: Nucl. Part. Phys. **40**, 105103 (2013).
[31] K. Yoshida, Phys. Rev. C **80**, 044324 (2009).
[32] J. Terasaki and J. Engel, Phys. Rev. C **84**, 014332 (2011).
[33] S. Ebata, T. Nakatsukasa, and T. Inakura, Phys. Rev. C **90**, 024303 (2014).
[34] I. Stetcu, A. Bulgac, P. Magierski, and K. J. Roche, Phys. Rev. C **84**, 051309(R) (2011).
[35] A. Tamii, T. Adachi, J. Carter, M. Dozono, H. Fujita, Y. Fujita, K. Hatanaka, H. Hashimoto, T. Kaneda, M. Itoh *et al.*, Nucl. Phys. A **788**, 53 (2007).
[36] Y. Fujita, B. Rubio, and W. Gelletly, Prog. Part. Nucl. Phys. **66**, 549 (2011).
[37] J. Birkhan, H. Matsubara, P. von Neumann-Cosel, N. Pietralla, V. Y. Ponomarev, A. Richter, A. Tamii, and J. Wambach, Phys. Rev. C **93**, 041302(R) (2016).
[38] R. M. Laszewski, R. Alarcon, D. S. Dale, and S. D. Hoblit, Phys. Rev. Lett. **61**, 1710 (1988).
[39] R. M. Laszewski, P. Rullhusen, S. D. Hoblit, and S. F. LeBrun, Phys. Rev. Lett. **54**, 530 (1985).
[40] R. M. Laszewski and P. Axel, Phys. Rev. C **19**, 342 (1979).
[41] R. M. Laszewski, R. J. Holt, and H. E. Jackson, Phys. Rev. Lett. **38**, 813 (1977).
[42] R. E. Chrien and W. R. Kane, *Neutron Capture Gamma-Ray Spectroscopy* (Springer-Verlag, New York, 1979).
[43] S. Raman, M. Mizumoto, and R. L. Macklin, Phys. Rev. Lett. **39**, 598 (1977).
[44] K. Sieja, Phys. Rev. C **98**, 064312 (2018).
[45] S. Maripuu, Nucl. Phys. A **123**, 357 (1969).
[46] D. Kurath, Phys. Rev. **130**, 1525 (1963).
[47] E. Migli, S. Drozdz, J. Speth, and J. Wambach, Z. Phys. A **340**, 111 (1991).
[48] S. Kamerdzhiev, J. Speth, G. Tertychny, and J. Wambach, Z. Phys. A **346**, 253 (1993).
[49] S. Moraghe, J. Amaro, C. García-Recio, and A. Lallena, Nucl. Phys. A **576**, 553 (1994).
[50] L. E. Marcucci, M. Pervin, S. C. Pieper, R. Schiavilla, and R. B. Wiringa, Phys. Rev. C **78**, 065501 (2008).
[51] L.-G. Cao, G. Colò, H. Sagawa, P. F. Bortignon, and L. Sciacchitano, Phys. Rev. C **80**, 064304 (2009).
[52] J. Speth, P.-G. Reinhard, V. Tselyaev, and N. Lyutorovich, arXiv:2001.07236.
[53] D. Vretenar, A. V. Afanasjev, G. A. Lalazissis, and P. Ring, Phys. Rep. **409**, 101 (2005).
[54] T. Nikšić, T. Marketin, D. Vretenar, N. Paar, and P. Ring, Phys. Rev. C **71**, 014308 (2005).
[55] N. Paar, D. Vretenar, E. Khan, and G. Colò, Rep. Prog. Phys. **70**, 691 (2007).
[56] N. Paar, D. Vretenar, T. Marketin, and P. Ring, Phys. Rev. C **77**, 024608 (2008).
[57] Y. Niu, N. Paar, D. Vretenar, and J. Meng, Phys. Lett. B **681**, 315 (2009).
[58] E. Khan, N. Paar, and D. Vretenar, Phys. Rev. C **84**, 051301(R) (2011).
[59] N. Paar, C. C. Moustakidis, T. Marketin, D. Vretenar, and G. A. Lalazissis, Phys. Rev. C **90**, 011304(R) (2014).
[60] X. Roca-Maza, N. Paar, and G. Colò, J. Phys. G: Nucl. Part. Phys. **42**, 034033 (2015).
[61] T. Nikšić, N. Paar, P.-G. Reinhard, and D. Vretenar, J. Phys. G: Nucl. Part. Phys. **42**, 034008 (2015).
[62] N. Paar, T. Marketin, D. Vale, and D. Vretenar, Int. J. Mod. Phys. E **24**, 1541004 (2015).
[63] D. Vale, T. Rauscher, and N. Paar, J. Cosmol. Astropart. Phys. 02 (2016) 007.
[64] X. Roca-Maza and N. Paar, Prog. Part. Nucl. Phys. **101**, 96 (2018).
[65] T. Nikšić, N. Paar, D. Vretenar, and P. Ring, Comput. Phys. Commun. **185**, 1808 (2014).
[66] E. Yüksel, T. Marketin, and N. Paar, Phys. Rev. C **99**, 034318 (2019).
[67] H. Pai, T. Beck, J. Beller, R. Beyer, M. Bhike, V. Derya, U. Gayer, J. Isaak, Krishichayan, J. Kvasil, B. Löher, V. O. Nesterenko, N. Pietralla, G. Martínez-Pinedo, L. Mertes, V. Y. Ponomarev, P.-G. Reinhard, A. Repko, P. C. Ries, C. Romig, D. Savran, R. Schwengner, W. Tornow, V. Werner, J. Wilhelmy, A. Zilges, and M. Zweidinger, Phys. Rev. C **93**, 014318 (2016).
[68] T. Nikšić, D. Vretenar, and P. Ring, Phys. Rev. C **78**, 034318 (2008).
[69] J. F. Berger, M. Girod, and D. Gogny, Comput. Phys. Commun. **63**, 365 (1991).
[70] N. Paar, P. Ring, T. Nikšić, and D. Vretenar, Phys. Rev. C **67**, 034312 (2003).
[71] T. Nikšić, D. Vretenar, and P. Ring, Phys. Rev. C **66**, 064302 (2002).
[72] E. Lipparini, S. Stringari, M. Traini, and R. Leonardi, Nuovo Cimento A (1965-1970) **31**, 207 (1976).
[73] H. Sagawa, G. Colò, X. Roca-Maza, and Y. Niu, Eur. Phys. J. A **55**, 227 (2019).
[74] W. G. Love and M. A. Franey, Phys. Rev. C **27**, 438 (1983).
[75] J. S. Dehesa, J. Speth, and A. Faessler, Phys. Rev. Lett. **38**, 208 (1977).
[76] J. Speth and A. van der Woude, Rep. Prog. Phys. **44**, 719 (1981).
[77] T. Suzuki, J. Phys. Colloques **45**, 251 (1984).
[78] K.-F. Liu, H.-D. Luo, Z. Ma, M. Feng, and Q.-B. Shen, Nucl. Phys. A **534**, 48 (1991).
[79] F. Osterfeld, Rev. Mod. Phys. **64**, 491 (1992).
[80] V. F. Weisskopf, Phys. Rev. **83**, 1073 (1951).
[81] P. Ring and P. Schuck, *The Nuclear Many-Body Problems* (Springer-Verlag, Berlin, 1980).
[82] K. Yako, M. Sasano, K. Miki, H. Sakai, M. Dozono, D. Frekers, M. B. Greenfield, K. Hatanaka, E. Ihara, M. Kato, T. Kawabata, H. Kuboki, Y. Maeda, H. Matsubara, K. Muto, S. Noji, H. Okamura, T. H. Okabe, S. Sakaguchi, Y. Sakemi, Y. Sasamoto,

K. Sekiguchi, Y. Shimizu, K. Suda, Y. Tameshige, A. Tamii, T. Uesaka, T. Wakasa, and H. Zheng, Phys. Rev. Lett. **103**, 012503 (2009).

[83] J. R. Tompkins, C. W. Arnold, H. J. Karwowski, G. C. Rich, L. G. Sobotka, and C. R. Howell, Phys. Rev. C **84**, 044331 (2011).

[84] Y. Tanimura, K. Hagino, and H. Sagawa, Phys. Rev. C **86**, 044331 (2012).

[85] D. I. Sober, B. C. Metsch, W. Knüpfer, G. Eulenberg, G. Küchler, A. Richter, E. Spamer, and W. Steffen, Phys. Rev. C **31**, 2054 (1985).

[86] A. Richter, A. Weiss, O. Haüsser, and B. A. Brown, Phys. Rev. Lett. **65**, 2519 (1990).

[87] G. F. Bertsch and I. Hamamoto, Phys. Rev. C **26**, 1323 (1982).

[88] M. Ichimura, H. Sakai, and T. Wakasa, Prog. Part. Nucl. Phys. **56**, 446 (2006).